Surface Science 254 (1991) 125–143
North-Holland

Kinetics of hydrogen oxidation to water on the Rh(111) surface using multiple source modulated molecular beam techniques

D.F. Padowitz [1] and S.J. Sibener

The James Franck Institute and The Department of Chemistry, The University of Chicago, Chicago, IL 60637, USA

Received 28 November 1990; accepted for publication 5 March 1991

We have examined the kinetics of the oxidation of hydrogen to water on the Rh(111) surface using modulated molecular beam reactive scattering. For reactant pressures below 10^{-4} Torr and temperatures from 450–1250 K we observe serial steps, with apparent activation energies of 2.5 ± 1 and 10 ± 1 kcal/mol. Pseudo-first-order preexponential factors are 10^5 and 10^7 s^{-1}, respectively, varying slightly with oxygen coverage. Reaction is inhibited by excess oxygen. Maximum water production occurs around 650 K. At lower temperatures the reaction becomes nonlinear. We use a new three-molecular-beam arrangement. Two continuous, independently adjustable beams establish steady-state surface concentrations, while a weaker modulated third beam induces small concentration perturbations around the selected steady state. With this technique we varied surface oxygen coverages, used isotopic substitution in the three beams to produce H_2O, D_2O and HDO, and linearized the HDO reaction.

1. Introduction

The formation of water by oxidation of hydrogen on transition metal catalysts is, by current standards, a complex reaction with many fascinating features. Hydrogen and oxygen are dissociatively chemisorbed on Rh(111) above room temperature. The kinetics of hydrogen adsorption are coverage dependent and strongly affected by oxygen coadsorption. Oxygen shows very involved behavior on the rhodium surface, such as island formation at low temperatures and dissolution into the bulk metal at high temperatures. At high temperatures water formation probably proceeds through sequential addition of hydrogen to oxygen with a hydroxyl intermediate; hydroxyl disproportionation may become important at low temperatures and high coverages. Hydrogen recombination, hydrogen reacting with hydroxyl, and hydroxyl disproportionation may each be second order in concentration. These second-order terms and the coverage dependence of sticking and desorption rate constants are likely to make the kinetics nonlinear, which greatly complicates analysis.

1.1. Mechanism

Simply for orientation, consider a mechanism for hydrogen oxidation consisting of the following elementary steps:

$$H_{2gas} \underset{k_{dH_2}}{\overset{s_0(1-([H]+[O]))^2}{\rightleftarrows}} 2H, \tag{1}$$

$$O_{2gas} \underset{k_{dO_2}}{\overset{s_0(1-[O])^2}{\rightleftarrows}} 2O, \tag{2}$$

$$O \underset{k_{surf}}{\overset{k_{bulk}}{\rightleftarrows}} O_{bulk}, \tag{3}$$

$$H + O \underset{k_{-1}}{\overset{k_1}{\rightleftarrows}} OH, \tag{4}$$

$$H + OH \underset{k_{-2}}{\overset{k_2}{\rightleftarrows}} H_2O, \tag{5}$$

$$2OH \underset{k_{-3}}{\overset{k_3}{\rightleftarrows}} H_2O + O, \tag{6}$$

$$H_2O \xrightarrow{k_{dH_2O}} H_2O_{gas}. \tag{7}$$

[1] Current address: Department of Chemistry, University of California, Berkeley, CA 94720, USA.

The first steps are dissociative adsorption and recombinative desorption. The terms s_0 are the sticking fractions at zero coverage. Coverage dependent adsorption is represented in the $(1 - [O])$ terms, which may be first order at low temperatures if there are molecular precursors; otherwise they are second order. Bulk solution of oxygen is represented by eq. (3). The rate parameters for hydrogen desorption, and perhaps others, are coverage dependent. Eq. (6) is OH disproportionation. The final step is the desorption of water.

This mechanism assumes no dissociation of water after formation. We have neglected any surface transport or diffusion terms. We do not consider multiple adsorption states. It is always possible that surface kinetics are dominated by reaction at particularly active defect sites. While many other complications are undoubtedly present, we will look at the simplest mechanisms that explain the observed kinetics.

1.2. Previous work

Water formation is of fundamental interest in heterogeneous catalysis and has been extensively studied. The earlier work is reviewed in ref. [1]. We will restrict our comments here to a few relevant studies on the (111) faces of Pt, Pd and Rh.

Engel and Kuipers looked at H_2O formation on Pd(111) [2]. A first-order response to H_2 pressure led them to believe that $H + O \rightarrow OH$ was rate limiting, with $E_a = 7$ kcal/mol and $\nu = 4 \times 10^{-8}$ cm^2 atom^{-1} s^{-1}. Diffusion of H between surface and bulk dominated the kinetics with excess H_2, but was blocked by excess O_2. They observed no difference in kinetics between hydrogen and deuterium oxidation. We obtain a similar apparent activation energy, but will offer a different analysis.

Direct evidence for adsorbed OH species on Pt(111) was given by Fisher and Gland in X-ray photoelectron spectroscopy (XPS) of coadsorbed water and oxygen [3]. Mitchell and White identified hydroxyl intermediates by high resolution electron energy loss spectroscopy (HREELS) of hydrogen oxidation on Pt(111) [4].

We are greatly indebted to a beautiful series of papers published in 1979 by Yates, Thiel and Weinberg. They used low-energy electron diffraction (LEED) and thermal desorption spectroscopy (TDS) to examine the adsorption [5,6], coadsorption [7] and reaction [8] of hydrogen and oxygen on Rh(111).

For H_2 adsorption they found second order Langmuir kinetics, $d\theta/dt \propto (1 - \theta)^2$, where θ is surface coverage. In the low coverage limit the sticking fraction s_0 was 0.65. The activation energy for second order desorption was $E_d^{(2)} = 18.6$ kcal/mol with pre-exponential $\nu_0^{(2)} = 1.2 \times 10^{-3}$ cm^2/s. These values varied strongly with coverage. No difference was observed between H_2 and D_2 kinetics [5]. Using a different technique we have duplicated the low coverage values [9].

Assuming second-order desorption for O_2, E_d was 56 ± 2 kcal/mol and $\nu = 2.5 \times 10^{-3}$ cm^2 s^{-1}. Auger spectra combined with TDS gave evidence of dissolution into the bulk above 400 K [6].

The effects of oxygen and hydrogen coadsorption were complex [7,10]. Oxygen coadsorption decreased the activation energy of hydrogen desorption. Oxygen precoverage blocked subsequent hydrogen adsorption, but oxygen did adsorb on a hydrogen covered surface to 80% of its saturation coverage for the clean surface. Only 7% of the oxygen thermally desorbed from the hydrogen precovered surface, perhaps indicating enhanced bulk solution. These points should be noted, as they may explain some of the more puzzling results of the present study.

LEED was used to follow reaction of the low-temperature (2×2) O layer with H_2 [8,11]. Oxygen was adsorbed on the cold surface, which was then exposed to hydrogen gas and heated until reaction occurred above 270 K. This reaction was first order in hydrogen pressure. The reaction with disordered oxygen was half order in P_{H_2}. Due to the time scale for LEED, depletion of the adsorbed layer, and dissolution, these experiments were limited to temperatures below 350 K, much lower than the reaction peak, which is around 600 K. An energy diagram for reaction of hydrogen with an ordered oxygen layer slightly above room temperature is found in ref. [11]. An apparent overall activation energy of 17.4 kcal/mol was obtained.

Gland, Fisher and Kollin titrated oxygen ad-

sorbed on Pt(111) at 300–450 K using 10^{-8} to 10^{-9} Torr hydrogen. Their results suggested sequential addition of atomic hydrogen to oxygen, with kinetics depending on the structure of ordered oxygen islands [12].

The evolution of OH below 165 K on oxygen-covered Pt(111) exposed to H_2 has recently been studied by Germer and Ho using high-resolution electron energy loss spectroscopy [13]. A model of molecular hydrogen precursors reacting at the edges of oxygen islands was proposed, with an activation energy of 2.8 ± 0.3 kcal/mol assigned to hydroxyl formation, and 4.2 ± 0.3 for water production.

Anton and Cadogan recently reported a molecular beam study using modulated oxygen in the limit of low reactant coverages on Pt(111). Activation energies of 16 and 18 kcal/mol were assigned to D + OD and OD + OD reactions [14].

These various values are not easily compatible. While it is possible that the analyses of some studies are flawed, it is clear that this reaction shows widely varying kinetics, and perhaps alternate mechanisms, in different temperature and coverage regimes.

1.3. New approaches

We explored hydrogen oxidation with a variety of techniques, the most important being modulated molecular beam reactive scattering or modulated molecular beam relaxation spectrometry (MBRS). In this method a periodic reactant flux produces a time dependent product flux, which is analyzed to extract the surface reaction kinetics. We use a new *three*-molecular-beam arrangement for linearized MBRS which increases the power and flexibility of the technique in unraveling complex kinetics. Two continuous, independently adjustable beams establish a steady state on the surface, while a weaker modulated third beam induces concentration perturbations around the selected steady state. In the limit of small perturbation by the modulated beam, the response becomes linear. We demonstrate this for HDO produced in the water reaction with hydrogen, deuterium, and oxygen beams, an arrangement shown in fig. 1. Control of steady state surface coverages is important for determining coverage dependent activation energies and pre-exponential factors. With the continuous beams we vary the

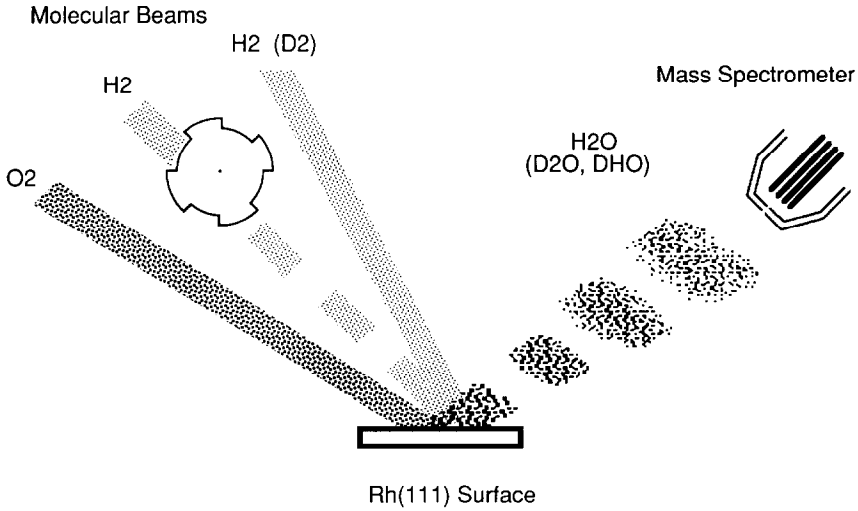

Fig. 1. Schematic of multiple molecular beam configuration. In addition to continuous oxygen and modulated hydrogen beams, a third continuous beam of hydrogen or deuterium was used to control surface coverages and linearize the reaction.

steady-state oxygen coverage on the surface and examine the rates. Finally, by controlling reactant and intermediate coverage regimes, we may be able to isolate individual elementary steps in complex reaction mechanisms.

A separate publication describes this new technique in detail [9]. In this paper we also employ several other complementary methods to give an overview of water formation on Rh(111).

2. Experimental

The surface scattering machine, fig. 2, was a removable source chamber containing three supersonic molecular beams and a main chamber with sample and manipulator, mass spectrometer detector, residual gas analyzer, Auger spectrometer and sputter ion gun. The base pressure in the scattering region was 5×10^{-11} Torr, rising to 6×10^{-9} Torr at the highest beam fluxes. The system has been described previously in refs. [15,16].

The source chamber had three regions of differential pumping before the main chamber. Each beam originated from an ~ 100 μm pinhole, was skimmed and collimated, then passed through a solenoid operated shutter. The center beam was modulated at 20–800 Hz by a chopper wheel with a four-slot 50% total duty cycle pattern, or a dual pattern chopper with two 25% slots and two 1% slits for time-of-flight measurements.

The distance from chopper to sample was 21.21 cm. Upon entering the main chamber the continuous side beams were defined by 80 mil apertures, the modulated beam by a 40 mil aperture. The left and right beams were 15° off axis, and the sample normal was usually at 45° resulting in roughly 5×7 mm elliptical spots on the sample, which overlap the center 2.5×3.25 mm modulated beam spot. Maximum side beam fluxes were on the order of 10 langmuir per second, or 10^{-5} Torr cm^{-2}.

The detector was a quadrupole mass spectrometer, doubly differentially pumped by two 60 ℓ/s ion pumps and an additional 50 ℓ/s turbo pump on the ionizer region. Acceptance angle of the detector was 1°. Flight path from sample to ionizer was 14.45 cm. At normal, the detector views a spot of ~ 2.5 mm diameter. The scattering center was the intersection of the molecular beam with the detector line of sight, and the detector

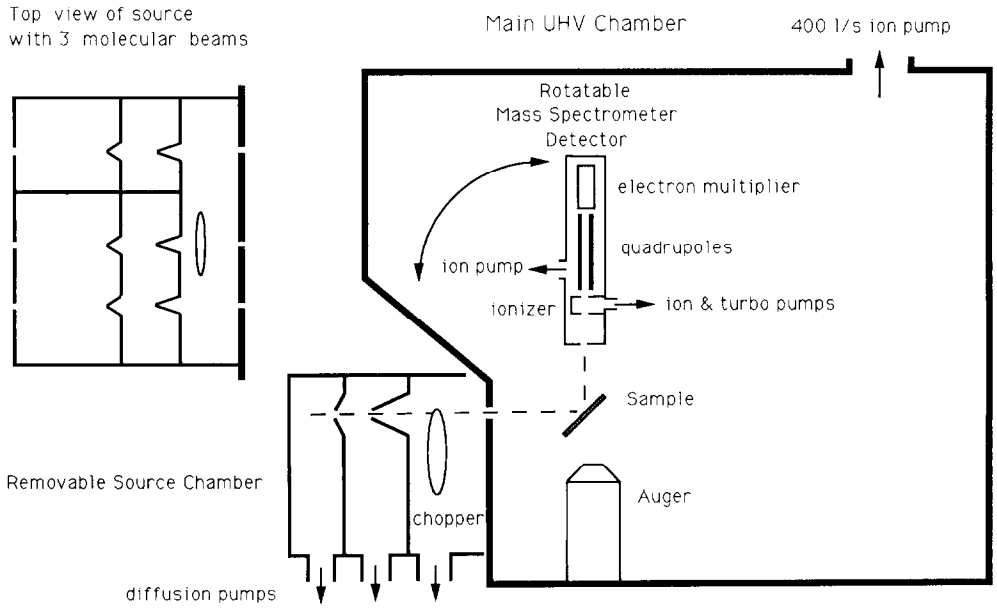

Fig. 2. Modulated molecular beam surface scattering apparatus. The system consists of a bakable stainless steel ultrahigh vacuum chamber and a removable source chamber.

rotated in the scattering plane defined by the center beam and the surface normal.

A rhodium single-crystal sample was cut and polished using standard techniques. The surface was within 0.5° of the fcc (111) plane, as determined by Laue X-ray diffraction. The Rh(111) surface is unrelaxed and unreconstructed, within 5% of the bulk lattice dimensions [11]. Auger spectra showed carbon, sulfur and boron contamination which was removed by cycles of argon ion sputtering (1.5 keV, 5 μA) and heating in $< 1 \times 10^{-5}$ Torr oxygen, following DeLouise et al. [17]. After the initial cleaning, Auger showed some carbon accumulation overnight, but this was rapidly removed by oxygen and hydrogen fluxes under reaction conditions. Due to the cycles of oxidation and reduction, the surface remained very clean during the course of experiments. Specular reflectivity of a 64 meV He beam from the room temperature surface was often better than 20%, indicating a low defect density.

The sample was resistively heated, and its temperature measured by a chromel–alumel thermocouple spot-welded to the back. Temperature could be maintained to ± 2 K by a feedback controller. Reactions were studied from 400–1200 K and the sample heated to 1250–1325 K for cleaning.

Data were collected with a lock-in amplifier, or in one of several computer-controlled modes. Time-of-flight (TOF) and diffraction modes used an LSI-11/23 compatible computer interfaced to a CAMAC system. Titrations or temperature and angle dependent yields were measured in diffraction mode using a gated integrator. Reaction product waveforms were taken in TOF mode with a custom multichannel scalar system. The scalar was triggered by a photodetector on the chopper wheel assembly. For TOF runs 255 channels of 5–20 μs were collected. For this reaction, good quality waveforms usually required 10–60 minutes of averaging.

3. Results

3.1. Reactant pressure dependence and reaction order

Reactant pressures at the surface were roughly 10^{-6}–10^{-5} Torr for hydrogen, and typically an order of magnitude lower for oxygen. A dose of one langmuir (1 L = 10^{-6} Torr · s) is approximately 10^{14} molecules cm^{-2} or roughly a monolayer (ML). We did not measure absolute reactant beam fluxes, but could obtain good relative flux calibrations based on the pressure rise in the chamber when the beams were scattered from a hot sample.

The rate of water production at 650 K was measured as a function of O_2 and H_2 beam pressures using lock-in detection with H_2 modulated at 100 Hz. The data are presented in fig. 3. Sections taken at constant O_2 flux show that the reaction increases rapidly with H_2 flux, then levels off, indicating a reaction order in H_2 less than one. At constant high H_2 flux, the response to O_2 flux is linear. At low H_2 flux however, the rate is not monotonic with O_2 flux. As O_2 pressure is increased the water production first rises, then declines to zero for high O_2 fluxes. No global

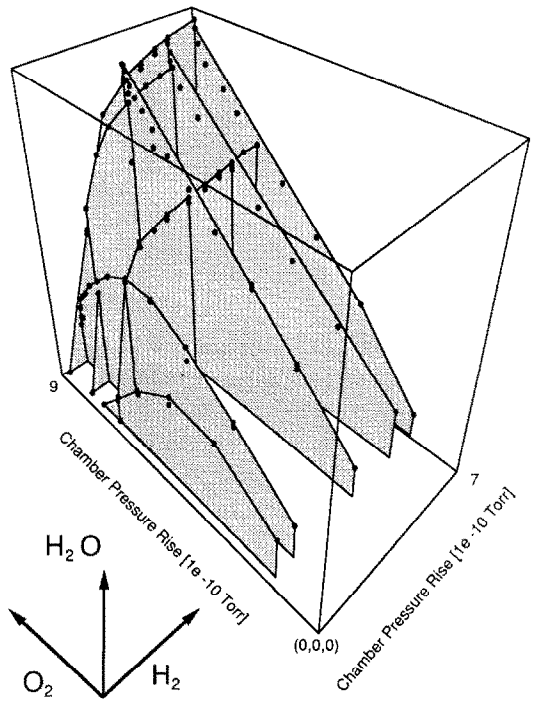

Fig. 3. Reaction order. Product mass spectrometer signal as a function of reactant beam flux around 650 K. Sections running from lower right to upper left are varying oxygen at constant hydrogen flux, the others vary hydrogen at constant oxygen flux. Note the complex behavior at low hydrogen pressures, seen in the left foreground.

reaction order can be specified in terms of reactant pressure. The reaction rate expression may be simpler in terms of surface concentrations, but these are not under direct experimental control. These data were measured under essentially steady-state conditions for which model mechanisms can be analyzed.

3.2. Steady-state calculation

At steady state the derivatives in the kinetic equations vanish. The set of simultaneous ODE's then reduces to a set of polynomial equations. These can usually be solved, unless they are of higher order than quartic. If so the roots may still be found numerically, though this can be difficult as it involves multidimensional minimization. Still, a solution may give little insight into the mechanism. Even a relatively simple kinetic model can rapidly become unwieldy. Consider the mechanism:

$$H_{2gas} \underset{k_{dH_2}}{\overset{s_0(1-[O])}{\rightleftarrows}} 2H, \tag{8}$$

$$O_{2gas} \xrightarrow{s_0(1-[O])} 2O, \tag{9}$$

$$H + O \underset{k_{-1}}{\overset{k_1}{\rightleftarrows}} OH, \tag{10}$$

$$H + OH \xrightarrow{k_2} H_2O. \tag{11}$$

For simplicity we use first-order Langmuir adsorption which should capture the essential coverage dependence without unduly complicating the calculations. Only oxygen coverage is included in sticking as the hydrogen coverage will be low. We also disregard oxygen desorption and assume no decomposition of H_2O. Subsuming the sticking coefficients into the reactant pressures, the rate equations are:

$$\frac{d[H]}{dt} = 2P_H(1-[O]) - 2k_d[H]^2 - k_1[H]\cdot[O] - k_2[H]\cdot[OH] + k_r[OH], \tag{12}$$

$$\frac{d[O]}{dt} = 2P_{O_2}(1-[O]) - k_1[H]\cdot[O] + k_r[OH], \tag{13}$$

$$\frac{d[OH]}{dt} = k_1[H]\cdot[O] - k_2[H]\cdot[OH] - k_r[OH]. \tag{14}$$

The steady-state solution for product flux is:

$$\frac{d[H_2O]_{gas}}{dt} = \left[k_d P_{O_2} \left(\frac{-2P_{O_2}}{k_1} + \sqrt{\frac{P_{H_2}}{k_d} - \frac{2P_{O_2}}{k_d} - \frac{2k_r P_{O_2}}{k_1 k_2} + \frac{P_{O_2}^2}{k_1^2}} \right)^2 \right] / \left[P_{H_2} - 2P_{O_2} \right]. \tag{15}$$

P_{H_2} and P_{O_2} are the reactant fluxes and incorporate the zero coverage sticking coefficients s_0.

We choose plausible values for the rate constants based on refs. [5,6,18]: $k_d = 7 \times 10^{-10}$, $k_1 = 4.5 \times 10^{-5}$, $k_2 = 2 \times 10^{-4}$, $k_r = 2 \times 10^{-8}$, scaled to units of monolayers and seconds. Using these numbers and our estimated reactant fluxes, we obtain fig. 4. This corresponds to the qualitative behavior of the experiment in fig. 3 quite well.

The asymptotic behavior is interesting. For high hydrogen flux the reaction is first order in oxygen and is nearly independent of hydrogen. We assume there is sufficient hydrogen and that the oxygen concentration is rate limiting. Steady-state water production at low hydrogen flux is more complicated. The initial slope in P_{H_2} may be linear, but soon drops below first order and perhaps saturates. The response to P_{O_2} at low P_{H_2} is most interesting, the rate first increases, then decreases to zero. Excess oxygen stops the reaction.

Eliminating the reverse reaction for OH by setting $k_r = 0$ in the previous result gives a plot identical to fig. 4. Thus k_r is not significant. On the other hand, the Langmuir sticking term $(1 - [O])$ in oxygen adsorption is essential. Without this factor we get the steady-state solution:

$$[OH] = \frac{2P_{O_2}}{[H]k_2}, \tag{16}$$

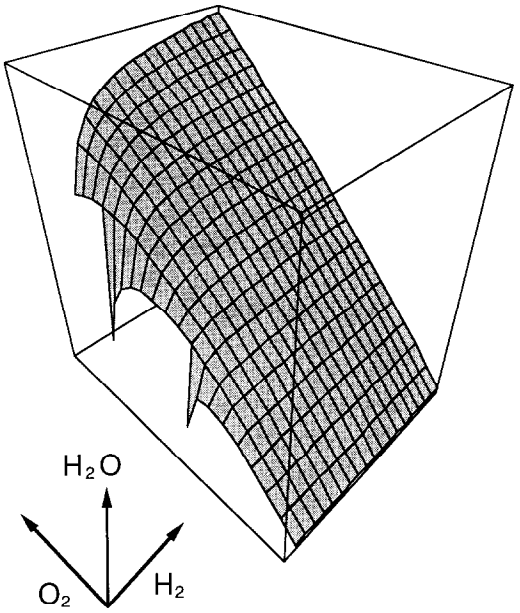

Fig. 4. Steady state calculation. Calculation generates the full surface, rather than the experimental sections of the previous figure. We match the essential qualitative features very well: nearly linear in P_{O_2} at high P_{H_2}, initial sharp rise then decreasing slope in P_{H_2}, and non-monotonic response to P_{O_2} at low P_{H_2}.

and thus

$$\frac{d[H_2O]_{gas}}{dt} = k_2[H]\cdot[OH] = 2P_{O_2}. \qquad (17)$$

Without saturation of O adsorption, water production depends only on P_{O_2} for any rate expression for hydrogen. This does not capture the very interesting behavior of the reaction at low P_{H_2}.

At high P_{O_2} : P_{H_2} ratios, we had thought that O blocked H_2 adsorption, but a Langmuir term for hydrogen sticking is not necessary in this model. Instead, we suspect that all the hydrogen is tied up as OH by the excess oxygen, so that none remains for the H + OH step. This is supported in the calculation by a large surface concentration of OH, but little H or H_2O production.

3.3. Titration of oxygen by hydrogen

In these experiments, the surface was first dosed with O_2 for a specific time, then the oxygen beam turned off. After a brief delay, the H_2 beam shutter was opened, and the H_2O production measured over time. The surface oxygen was thus "titrated" by H_2. Several titration runs are shown in fig. 5. For small O_2 doses water production is prompt. For larger doses, there is a small initial transient, and a slow rise to peak H_2O production. This induction time may indicate blocking of H_2 adsorption by oxygen. Or the induction period may be due to all the hydrogen being tied up as OH by the excess oxygen, which we believe was shown in the previous simulation. In any case, the excess oxygen must be removed before the maximum rate is reached.

3.4. Angular distribution

The angular distribution of the H_2O flux is cosine, and time-of-arrival waveforms are independent of angle. This is an indication that the product is equilibrated with the surface prior to desorption. We have assumed in all subsequent waveform analyses that H_2O desorbs with an equilibrium velocity distribution corresponding to the temperature of the surface. A more direct proof would require modulation of the product flux with a post-chopper between sample and detector.

In general, desorbing product need not be in equilibrium with the surface. In the case of CO_2 formed by the oxidation of CO, the product desorbs with a peaked angular distribution and with significant translational excitation [16]. In that

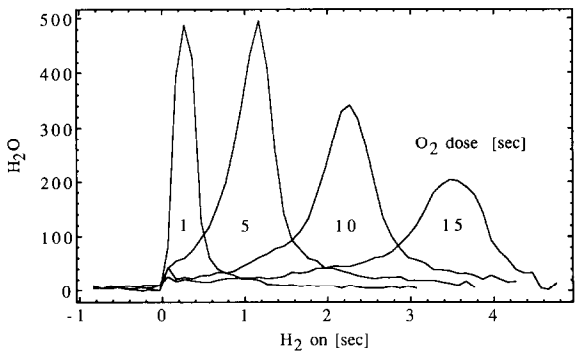

Fig. 5. Titration. After dosing the surface with oxygen, the hydrogen beam is turned on and water production observed. The dosing rate is ≤ 0.1 ML/s. Note that the reaction is prompt for lower oxygen doses, but higher doses delay the reaction peak.

reaction the transition state lies 12 kcal/mol above gas-phase CO_2 and the adsorption well is very shallow, so that the hot product does not remain on the surface long enough to equilibrate. Water may be formed with a very large amount of energy – the transition state for H + OH may lie as much as 35 kcal/mol above gas-phase H_2O. If the desorbed molecules are thermalized with the surface, it may be that the 10 kcal/mol adsorption well for H_2O is able to trap the excited product molecules.

3.5. Temperature dependence

Water production versus temperature from 450–1300 K is shown in fig. 6. There is a rapid rise to maximum reaction rate around 600 K and a gradual decrease with significant rates at the highest temperatures measured. This data set was taken in diffraction mode, in which the H_2 beam was chopped at low speed, about 175 Hz, and signal and background acquired with a gated integrator. Demodulation of the waveform introduced some error as signal leaked into the background period, causing a slightly too rapid decrease at low temperature. An essentially equivalent plot was obtained using a lock-in amplifier.

This peaked shape is typical for surface reactions. Low temperature throughput is limited by adsorption on the saturated surface. Above the maximum temperature yield decreases due to competition between reaction and desorption, which reduces the surface coverage of reactants.

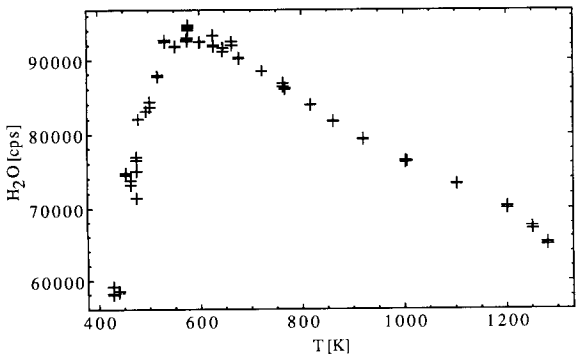

Fig. 6. Temperature dependence of reaction yield; $H_2 + \frac{1}{2}O_2 \rightarrow H_2O$/Rh(111). The plot shows the typical peaked shape of surface reactions. The maximum reaction rate is near 600 K. Above the peak, desorption of reactants competes with product formation.

Several previous studies have been done at temperatures below 300 K, where the reaction rates are low enough to be accessible to LEED or EELS measurements [8,11,13]. Where not specifically mentioned in our experiments, temperatures may be assumed to be in the region 650–665 K, near the reaction peak.

3.6. MBRS

Since the coverages of reactants change with temperature, the preceeding steady state measurements are not adequate to determine rate constants. It is necessary to turn to dynamic methods such as MBRS, in which the response to a time varying reactant flux is measured. A modulated reactant beam provides a fast "pressure jump" at the surface, and the rate at which the product flux responds is analyzed. Modulation of the product signal also greatly enhances signal to background discrimination. With the mass spectrometer we typically measure the time dependent water flux from the reaction of a continuous oxygen beam and chopped hydrogen beam. The multichannel scalar is triggered at each chopper pulse and the "time-of-arrival" distribution of the product at the detector is averaged over many chopper cycles.

Time-of-arrival waveforms at 665 and 568 K are shown in fig. 7. As a first approximation, the differing slopes reflect a temperature dependent surface "residence time" for the reaction. The time constant for a single exponential fit to the decay is τ. Assuming a single-step first-order reaction, τ would be the inverse of the first-order rate constant: $k = 1/\tau$ and so $\ln \tau = -\ln k$.

3.7. Single-step Arrhenius plots

A plot of $\ln \tau$ versus $1/T$ is shown in fig. 8. We have collected data over the wide temperature range 450–1200 K. At both extremes the signal level is low, as was seen in fig. 6, and the experimental error increases. Between 500 and 800 K the reaction exhibits approximately Arrhenius behavior. While the activation energy, indicated by the slope, is constant in this region, there is a sys-

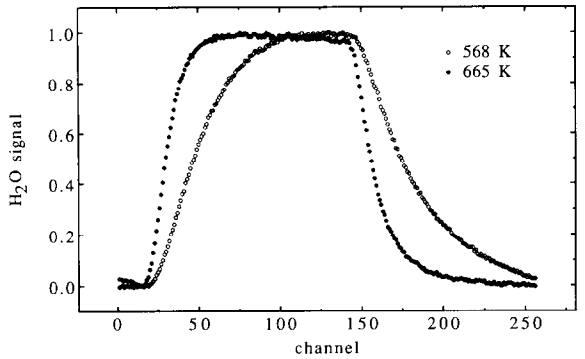

Fig. 7. Kinetic information is obtained from the temperature dependence of the product waveforms. The phase lag, seen in the slower rise and fall at lower temperature, indicates a longer "surface residence time" or lower reaction rate. More detailed information will be extracted by transfer function analysis.

tematic variation in pre-exponential factor. With analysis as a single step, we obtain $E_a = 6.8 \pm 0.4$ kcal/mol, and $A = 10^6$ to 10^7 s^{-1}. The authors of ref. [2] obtained 7 kcal/mol with the second-order pre-exponential 4×10^{-8} cm^2 $atom^{-1}$ s^{-1} for Pd(111). However, our analysis of the full transfer function will suggest a serial mechanism of two or more steps. The actual activation energies will therefore differ from these apparent values. This point and the variation of the pre-exponential will be examined in more detail later.

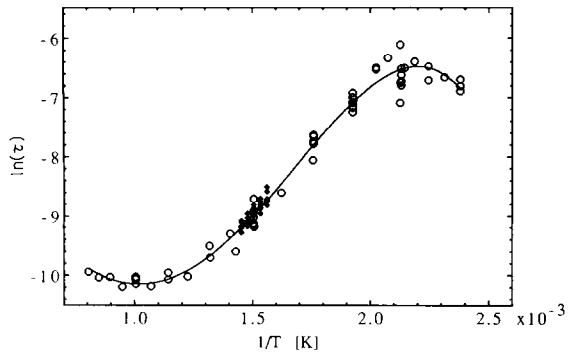

Fig. 8. Pseudo-first-order Arrhenius plot. For a single step reaction $\tau = 1/k$. The solid line is a polynomial fit only to indicate the trends. The slope is constant over a wide temperature range with an effective or pseudo-first-order activation energy of 6.8 kcal/mol. The error increases at the ends, but the scatter in the central region is systematic, and greater than experimental uncertainty.

3.8. *Transfer function analysis of linear surface kinetics*

A simple exponential fit, or equivalently measuring the phase lag at one frequency with a lock-in, is sufficient only for a single first-order reaction step. To obtain more complete kinetics for complex reactions we analyze the full waveform. Using Fourier transform deconvolution, we determine the phase and amplitude of the product signal for each frequency component in the modulated reactant beam. This gives the frequency-domain impulse response of the system or the "transfer function". Transfer functions have characteristic forms for different simple linear reaction mechanisms, from which rates can easily be extracted. Derivation of transfer functions from modulated beam data has often been discussed, see ref. [9] and references therein.

3.9. *CO_2 and H_2O transfer functions*

Fig. 9 compares transfer functions for carbon monoxide oxidation $CO + O_2 \rightarrow CO_2$ and for hydrogen oxidation $H_2 + O_2 \rightarrow H_2O$, both on the

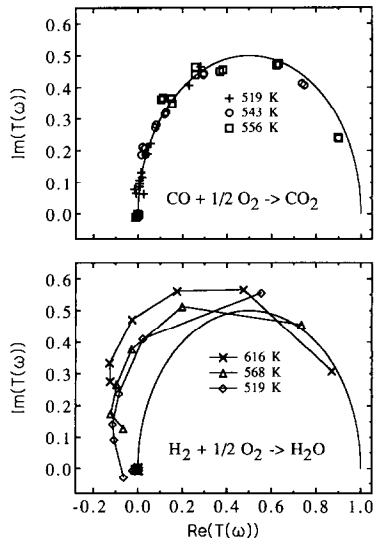

Fig. 9. Transfer functions for CO_2 and H_2O. Carbon monoxide oxidation on Rh(111) is first order in CO, and the transfer function is a semicircle. Under similar conditions, H_2O formation is not a single first-order step, but a serial mechanism. The rate ratios vary with temperature.

Rh(111) surface over a similar temperature range. The CO_2 reaction is effectively first order in CO, perhaps because an excess flux of O_2 maintains a saturation coverage of atomic oxygen [16]. Hydrogen oxidation cannot be similarly reduced to first order, since excess oxygen throttles the reaction. The transfer function for CO_2 is the semicircular arc characteristic of a single rate-limiting step. Changes in surface temperature or beam modulation frequency simply rotate the points along the arc. H_2O is not a single step, but shows the pattern of a serial mechanism.

3.10. Nonlinearity

Transfer function analysis is straightforward only if the product responds linearly to changing reactant [19]. Nonlinearity prohibits experimental deconvolution and the use of transform analysis methods, and frequently presents severe mathematical difficulties in analyzing chemical reaction mechanisms. Unfortunately, chemical systems are rarely linear. An elementary bimolecular step in a chemical reaction involves two species and the rate of reaction depends on the product of their concentrations. If both concentrations change with time, the mechanism will be nonlinear. A reaction will also be nonlinear if the rate constants change with concentration. This is frequently true for surface reactions, because adsorption probabilities, pre-exponential factors and activation energies often depend on coverages. All of these factors are present in the mechanism for water production outlined above, eqs. (1)–(7).

Whether these mechanistic nonlinearities will be evident in a particular experiment depends on coverage and the actual values of the rate constants. Above the peak temperature of 600 K we see approximately linear responses over the accessible range of reactant pressures. The rise and fall of the waveforms show only slight asymmetry, the transfer function is independent of chopper frequency, and the even harmonics are small. At lower temperatures however, the reaction does become strongly nonlinear. The presence of even harmonics in the Fourier transform beyond experimental noise indicates nonlinear kinetics. This is the case for H_2O at low temperatures, as seen in fig. 10.

3.11. Lower surface temperatures

At temperatures above 600 K, though it is not a single-step process, the reaction is effectively linear. Below 520 K, the reaction is significantly nonlinear, as shown above. At even lower temperatures the signal becomes erratic, depending on the history of beam fluxes and surface temperatures. We suspect that at low temperatures the oxygen coverage would grow in between chopper pulses, and that reaction stopped if the surface was allowed to saturate with oxygen. This is consistent with our steady state model showing a drop in reaction rate for excess oxygen. It is also in accord with the titration experiments which, if the initial oxygen dose was large, showed an induction period for H_2O after the hydrogen beam was turned on.

3.12. Coverage dependent kinetics: multiple beams

To examine the reaction over a wide range of surface coverages we will use multiple reactant

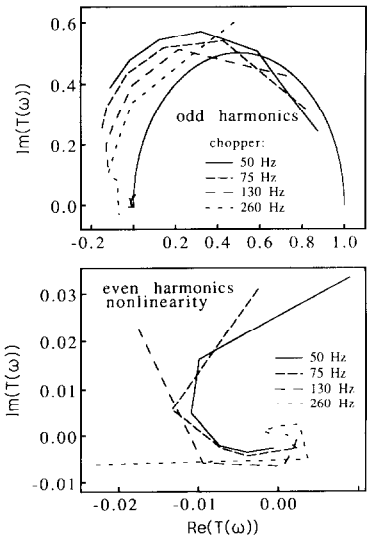

Fig. 10. H_2O nonlinearity. At low temperatures the H_2O transfer function varies with modulation frequency, evidence of a nonlinear response. Clearer evidence is the presence of even harmonics in the output, which are not present in the square wave modulated input.

sources and linearized MBRS methods. With a continuous hydrogen beam in addition to continuous oxygen and modulated hydrogen beams, we can to some extent control the hydrogen-to-oxygen ratio on the surface. For instance, a continuous hydrogen flux prevents oxygen saturation between chopper pulses of modulated hydrogen. This greatly increases the signal for low surface temperatures, as shown in fig. 11 at 465 K. That this is possible again demonstrates that the response to hydrogen flux is not linear. If it were, the modulated product response would be independent of the additional continuous hydrogen flux. Next we show waveforms at 495 K with and without a continuous hydrogen flux. The waveform with the continuous beam shows a slower response. Not only is the total reaction yield nonlinear, but the kinetics vary as well. To see whether oxygen coverage affects the rate constants or alters the mechanism, we can use the three-beam method to explore the reaction at different oxygen coverages.

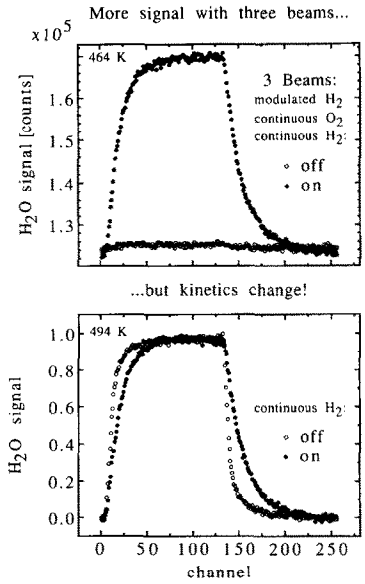

Fig. 11. Coverage dependent kinetics at low temperature. The use of three beams, modulated hydrogen, continuous oxygen, and continuous hydrogen, greatly increases signal levels and reveals coverage dependent kinetics.

But first we will consider oxygen adsorption on Rh(111).

3.12.1. Oxygen adsorption

Over the temperature range of this work, 400–1000 K, oxygen dissociatively chemisorbs on the Rh(111) surface. Though well studied, this system is complex and not fully understood. Thiel et al. [6] report that oxygen adsorbs in a disordered state at 100 K, orders irreversibly to a (2×2) structure above 150 K, and disorders again above 280 K. There are two TDS peaks, at 840 and 1125 K [20]. There is evidence for dissolution of oxygen into the bulk Rh above 400 K [21]. This bulk diffusion may have a significant effect on surface oxygen coverage and other reaction kinetics. This system is also described in ref. [11].

The oxygen coverage may be measured by Auger spectroscopy. The Rh peaks also vary with oxygen coverage and temperature, so the O/Rh peak ratio is used to measure oxygen coverage. Oxygen adsorption isotherms indicate second-order Langmuir adsorption. Assuming a saturation coverage of about 0.8 and a sticking coefficient of $s_0 = 0.1$, the initial slope of our isotherms give a typical dosing rate of about 0.1 L/s.

A slow decrease of oxygen coverage is observed at temperatures below the onset of desorption. When the Auger spectrometer is on, part of the decrease is probably due to desorption stimulated by the electron beam. At 650 K desorption is insignificant, so that dissolution and processes due to the electron beam may dominate. The oxygen decrease at this temperature exhibits an unusual half-order decay. At 900 K the thermal desorption of O_2 will be significant. We expect a second-order process, but these conditions show a first-order decay. This may mean that recombinative O_2 desorption occurs at defects that remain saturated with oxygen, or that the decrease in coverage at this temperature is due largely to dissolution of oxygen atoms into the bulk Rh.

Heating to 1200 K or reaction with H_2 generally removes the oxygen, though we sometimes observe a small residual Auger oxygen peak which is only removed by heating to 1325 K. This is presumably dissolved O or a very tightly bound

species. We do not yet understand the formation of this state or know if it affects reaction kinetics.

3.12.2. Modulated oxygen kinetics

If the oxygen beam is modulated we see very slow changes in water production. Even at our lowest chopper frequencies, the waveform does not return to baseline between oxygen pulses. These demodulated waveforms are difficult to analyze, and we have not extracted the rates. We suspect this slow process corresponds to oxygen desorption kinetics. Waveforms for modulated oxygen and modulated hydrogen are compared in fig. 12. Despite the fast response to hydrogen modulation, we cannot rule out slower steps in water formation. We will return to this point in our discussion of possible mechanisms.

For most of our experimental conditions, it is reasonable to assume a constant oxygen coverage on the time scale of hydrogen modulation, but that long-term shifts in coverage can occur even under constant conditions. Our group is continuing to explore the kinetics of oxygen on Rh(111) in greater detail [21].

3.12.3. Coverage dependent rate constants

In the next set of experiments we exploit the additional control over reactant coverage made possible by three beams in linearized MBRS. The two continuous beams were used to vary the steady-state surface coverages, while the response to the modulated beam was recorded as a function of temperature, and multiple rates extracted by

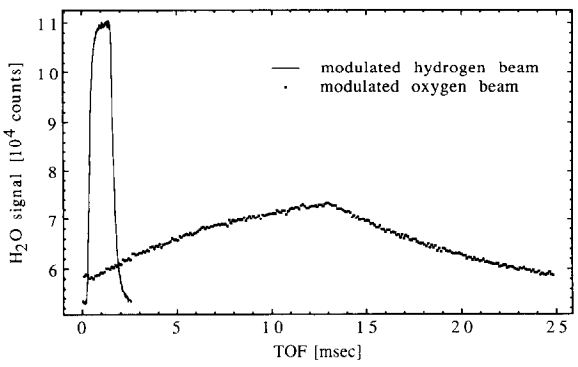

Fig. 12. Modulated oxygen and modulated hydrogen. Water production responds much more slowly to modulated oxygen.

transfer function analysis. The oxygen coverage, modulated H_2O and H_2O background all depend on the continuous hydrogen flux. We focus on oxygen coverage as it can be easily determined by Auger spectroscopy. Perhaps more importantly, the two continuous beams control the hydrogen to oxygen ratio, and the amount of hydroxyl intermediate on the surface, which we could not directly measure.

Auger spectra to measure oxygen coverage could not be taken simultaneously with mass spectrometer waveforms of water production, but it was possible to move between the two measurements in such a fashion that the surface conditions were unaltered. The crystal was placed in Auger position, inclined 45° to the incident beams. The flux in the continuous beam of H_2 was set and the steady-state oxygen coverage measured by Auger. Rotating the crystal 90° placed it in scattering position, again at 45° to the beams. Note that the beam fluxes, geometry and surface temperature are identical for both waveform and Auger measurements. Waveforms were taken at several temperatures over the narrow range 640–690 K. At the end of the temperature scan, the crystal was returned to Auger position and the oxygen coverage measured. The continuous beam flux was then changed, and the procedure repeated for the new steady state.

Transfer function analysis of the waveforms showed a nearly linear, multiple-step reaction for this regime, as in fig. 9. The transfer functions were then fit to a two-step serial process, yielding two rates for each run. Fig. 13 is an Arrhenius plot for these two rates at each steady state beam flux and temperature. The slopes of each set are roughly constant, giving activation energies of 10 and 2.5 kcal/mol, independent of oxygen coverage. The respective intercepts give pre-exponentials on the order of 10^7 and 10^5 s^{-1}.

The preexponential factors show a small but systematic variation with oxygen coverage. For an elementary step involving oxygen we would expect to measure an apparent first order response to modulated hydrogen with the constant oxygen coverage multiplying the true second-order pre-exponential, $k^{(1)\prime} = k^{(2)}[O]$. The pseudo-first-order pre-exponential will then vary linearly with oxygen

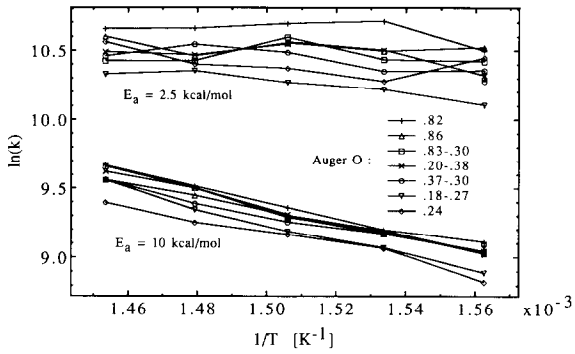

Fig. 13. Coverage dependent serial Arrhenius plot. Two series rates, extracted from the transfer function, shown as a function of both temperature and oxygen coverage. Activation energies are relatively constant, pre-exponentials appear to vary in a systematic fashion with oxygen coverage. Oxygen coverages were not stable.

coverage and vanish as the coverage approaches zero. This does not appear to be the case. If the reaction step does not directly include oxygen, dependence on oxygen coverage implies a more subtle effect on the surface dynamics.

In spite of the care taken that steady state had been reached and of the symmetry of the Auger and scattering positions with respect to the incident beams, the oxygen coverage sometimes varied substantially during a run. This again suggests some slow oxygen kinetics which were not well controlled, such as diffusion into the metal, or a surprising sensitivity to small changes in beam flux. Though some model mechanisms predict steady states that are unstable toward oxygen saturation of the surface, we would expect such instability to occur on the millisecond time scale seen in the modulated beam response, not over tens of minutes.

3.13. Oscillations

Oscillations in surface catalytic reactions have been observed by Ertl and coworkers during oxidation of carbon monoxide on the Pt(100) and (110) surfaces [22]. That reaction may also exhibit deterministic chaos via period doubling. To observe oscillation in a surface reaction requires coherent concentration fluctuations across the surface. This depends on diffusion, surface phase transition, or other long-range effects. The mechanism for oscillation on Pt crystal faces appears to be an adsorbate-induced surface phase transition: the CO coverage builds up until it induces a surface reconstruction, which then alters the reaction rates.

The Rh(111) surface does not reconstruct. The water reaction would seem to be sufficiently complex to support oscillatory behavior, if diffusion or other long-range factors can create phase coherence across the surface. We have two observations of fluctuations in oxygen coverage, but we could not reproduce this behavior at will.

Fig. 14 shows oxygen coverage as the hydrogen flux was varied under normal reaction conditions around 660 K. We took repetitive 30 s Auger scans through the oxygen peak. Initially we had low oxygen coverage due to a high hydrogen flux. The hydrogen was reduced, and the oxygen cover-

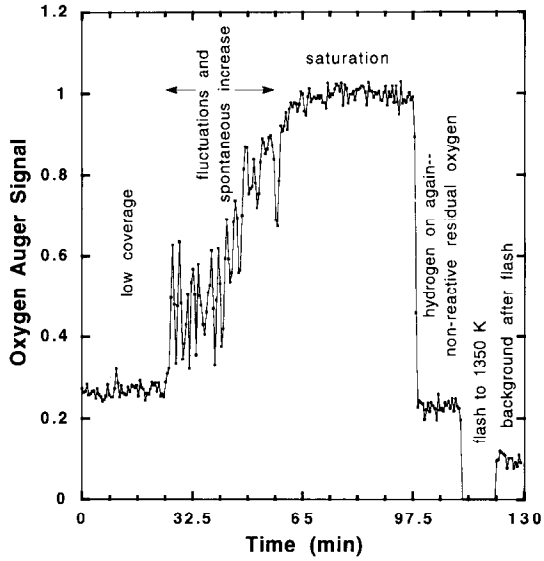

Fig. 14. Oscillations? Continuous Auger scans of the oxygen peak covering about 2 h. The beams were not modulated. Moving from left to right, the hydrogen flux was initially high, and the oxygen coverage low. The hydrogen flux was then lowered to allow partial coverage of oxygen to form. The intermediate oxygen coverage appears to have greater fluctuations than either low coverage or saturation, and spontaneously increased to near saturation over a 30 min period. The hydrogen was then turned off, and oxygen allowed to saturate, finally removed by a high hydrogen flux. Some residual oxygen could only be removed at high temperature.

age increased to roughly half saturation. However, the fluctuations here appear greater than at either the lower or higher coverages. The oxygen coverage spontaneously increased toward saturation over a period of 30 min. Hydrogen was then briefly increased to check that the reaction would respond, then turned off and the oxygen allowed to saturate. Noise or instrumental variation in the Auger signal should be greatest at high or low signal levels, depending upon its origins. That the largest fluctuations are seen at intermediate levels suggests that the variation is in fact due to oxygen coverage changes on a scale of a few minutes. We have never observed instabilities of this order in the molecular beam fluxes.

Long-term instability of oxygen coverage was also seen in the coverage dependent Arrhenius plot experiments. We did not obtain a power spectrum. At these temperatures we observe water production rates on the order of milliseconds. These cannot account for rate variations on a time scale 10^5 slower. Only the thermal desorption of oxygen and its dissolution into the bulk are this slow. If oxygen dissolution has a long-range effect on surface reactivity, this may be a new mechanism for kinetic oscillations in surface catalysis [23].

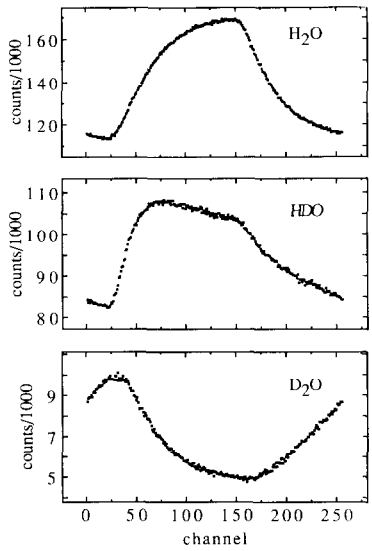

Fig. 15. Isotopic substitution. The three isotopic water waveforms produced with modulated hydrogen, continuous oxygen, and continuous deuterium beams. The H_2O waveform is as usual, the HDO waveform asymmetric, and the D_2O waveform inverted! Note that both deuterium and oxygen are not modulated, and so the modulation of D_2O is an indirect effect due to the perturbation of surface O or D by the modulated hydrogen flux.

3.14. Isotopes and linearization, $H_2 + D_2 + O_2$

We now show some remarkable results using isotopic substitution in three beams. When a continuous beam of D_2 is used along with a continuous beam of O_2 and modulated H_2, three isotopic forms of water are produced. Our hope was to isolate the H + OD step using large continuous fluxes of oxygen and deuterium to saturate the surface with OD. We would then examine the HDO produced by a small modulated hydrogen beam.

Initially, we used a large modulated H_2 flux, and obtained waveforms for the three products shown in fig. 15. The H_2O waveform has the usual symmetric form. The HDO product however, shows a highly asymmetric waveform, with a rapid rise, sloping top, and long decay. The D_2O wave is very interesting since neither the O_2 nor D_2 beams were modulated. This should produce a continuous background D_2O flux. The negative modulation must be induced indirectly by the chopped H_2 beam. The modulated flux is perturbing the steady state surface coverages and the depression of D_2O production is a direct measure of this perturbation.

A more complete description of the origin of these waveforms is presented in ref. [9]. The essential point is that the modulated beam is driving the system into nonlinearity. We wish to reduce the intensity until the modulated beam does not perturb the steady state coverages of reactants and intermediates. In this limit the HDO production will be linear. We can reduce the perturbation to 0.6% measured as variation in the steady-state D_2O evolution. To obtain good data at this level is a challenge, requiring several hours of signal averaging per waveform.

3.15. Mechanisms

3.15.1. Serial H_2O, HDO rate constants

Transfer functions for H_2O and approximately linearized HDO are shown in fig. 16. The curve for H_2O distinctly shows a serial process. The shape of the transfer function depends on the ratio of the serial rate constants, which vary with temperature. As shown earlier, the temperature dependence of the two steps gave an activation energy of 10 kcal/mol and a pre-exponential of 10^7 s^{-1} for one step and 2.5 kcal/mol with 10^5 s^{-1} for the other. The transfer function for approximately linearized HDO is closer to the single step arc, but additional steps are still evident. We obtain one rate with $A = 10^7$ s^{-1} and $E_a = 9.6 \pm 0.8$ kcal/mol, and a second rate with a similar pre-exponential but $E_a = 5.4 \pm 1.6$ kcal/mol. There is no difference between modulated H_2 and modulated D_2. How should we interpret these rate constants?

3.15.2. An oversimplification

Initially, suppose that the first of the serial steps in the H_2O reaction is $H + O \rightarrow OH$ and the second is $H + OH \rightarrow H_2O$. For HDO the second step might dominate: by using continuous beams of D_2 and O_2 we saturate the surface with OD, and then use the modulated H_2 beam to produce HDO. Thus we might isolate the $H + OD \rightarrow HDO$ step. At 665 K the H_2O transfer function can be fit with two steps with a 3 : 1 ration in rates. For HDO the ratio is 15 : 1, which more closely approaches a single step.

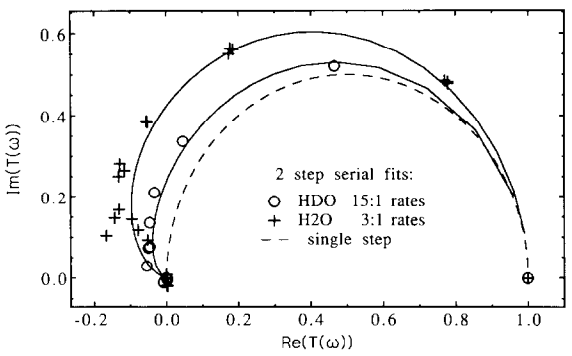

Fig. 16. Serial fits for H_2O and HDO. The shape of the transfer function for serial steps depends on the ratio of the rate constants. At 665 K, H_2O shows two steps with 3 : 1 rate constant ratio. For linearized HDO the ratio is 15 : 1.

Unfortunately, this simple scheme can not consistently assign activation energies to H + O and H + OH steps. For H_2O, we might suppose the 10 kcal/mol activation energy corresponds to H + O, and 2.5 kcal/mol to H + OH. But the single-step fit to HDO gives 6–8 kcal/mol, which does not match either number for H_2O. This is not an isotope effect; modulated D_2 and H_2 give identical results. Furthermore, if the serial steps in H_2O were H + O and H + OH, we would expect quadratic terms in [H], and nonlinearity. While H_2O was significantly nonlinear for temperatures below 520 K, the waveforms at 665 K had only minor nonlinearity.

The linearity of the reaction near the peak temperature mitigates against significant H + OH or OH + OH rates, which would introduce quadratic terms, unless OH coverage remains nearly constant over the modulation period. The transfer function does not show significant parallel reactions as would be the case if both H + OH and OH + OH contributed substantially to water production.

3.15.3. A caveat

The simple idea of a rate-limiting step may be misleading. Though we measure water waveforms, the observed rates need not depend only on reaction steps leading directly to water formation. Parallel processes which compete with product formation can also affect the product waveform and the measured rates. Typically this occurs if the branching ratio for reaction is low compared to desorption. For instance, the slow modulated oxygen waveforms do not necessarily imply slow kinetics in water formation. If water formation is a minor pathway for oxygen removal compared to desorption, oxygen adsorption–desorption kinetics will control oxygen coverage. Despite large rate constants, the overall rate of water formation could be limited by hydrogen coverage. The time dependent water formation will then be proportional to the slowly changing oxygen coverage. If there were excess hydrogen coverage on the surface, the modulated oxygen might then rapidly react, giving kinetics comparable to those measured with mod-

ulated hydrogen. Such conditions were unobtainable with available hydrogen beam fluxes.

Conversely, the fast response of water production to modulated hydrogen does not rule out slower steps, provided all intermediate concentrations rapidly follow hydrogen coverage.

Other processes which might appear in the observed rates are hydrogen recombination and water desorption. From ref. [11], water desorption has an activation energy of 10 kcal/mol, and would be present for both H_2O and HDO reactions. The cosine angular distribution of water indicates equilibration, and might imply a significant residence time. However the 10^7 s^{-1} pre-exponential is low for a first-order process. The 10^5–10^7 s^{-1} pre-exponentials for all the rates we have measured are consistent with second-order processes for low surface coverage. In ref. [9] we found 10 kcal/mol and 10^7 s^{-1} for linearized HD recombination, identical to one step in both H_2O and HDO. The apparent linearity for this process seems to imply a significant steady state coverage of hydrogen. This is surprising and suggests a reservoir of hydrogen perhaps from OH dissociation.

If the 10 kcal/mol step is hydrogen recombination, that leaves the 2.5 kcal/mol step as an apparent rate for O + H and H + OH. If H + O were rate limiting, the pseudo-first-order pre-exponential should vanish in the limit of zero oxygen coverage. This is not the case, though it does vary with oxygen coverage. If this step were H + OH, we would expect little change in the case of HDO, but we do find a somewhat different activation energy of 5 kcal/mol. The measured rates are reasonable magnitudes for diffusion to defects, but we do not see the characteristic transfer function for such processes.

We might try fitting the H_2O transfer function to three steps. In fact we expect this to give a slightly better fit to the data, but the rate constants so extracted will have poor statistics and may not be unique, so we have not followed this avenue.

3.15.4. An overcomplication

It is not possible in general to find analytic solutions for nonlinear mechanisms. We can however solve models for reactions such as HDO which have been experimentally linearized. For these reactions the effective or pseudo-first-order rate constants will differ from the true constants. Consider a very simple mechanism, with constant oxygen coverage and no reverse reactions:

$$H_{2gas} \overset{s}{\underset{k_d}{\rightleftarrows}} 2H, \tag{18}$$

$$H + O \xrightarrow{k_1} OH, \tag{19}$$

$$H + OH \xrightarrow{k_2} H_2O, \tag{20}$$

with the equivalent deuterium and mixed steps, for which we assume identical rates. In the linear limit of a small modulated flux of H_2 and a large continuous background of D_2, or vice versa, we obtain the transfer function:

$$T(\omega) = \frac{1}{2}\left(\frac{1 + i(\omega/k_h)}{1 + (\omega/k_h)^2}\right)\left(1 + \frac{1 + i(\omega/dk_2)}{1 + (\omega/dk_2)^2}\right). \tag{21}$$

This is not a single step, but corresponds to a linear combination of serial and parallel steps with effective rates:

$$k_h = 2k_1[O] + dk_d, \tag{22}$$

$$d = \frac{-2k_1[O] \pm \sqrt{4(k_1[O])^2 + 16sp_0k_d}}{4k_d}. \tag{23}$$

Suppose desorption greatly exceeds reaction: $k_d \gg k_1[O]$. The apparent rates become $k_h = \sqrt{sp_0k_d}$ and $dk_2 = k_2\sqrt{sp_0/k_d}$. From the observed activation energy, $E_h = 10$ kcal/mol = $E_d/2$, so hydrogen desorption is 20 kcal/mol and then $E_{dk_2} = 5$ kcal/mol $= E_2 - E_d/2$ and H + OH is 15 kcal/mol. To determine the rates k_1 and k_2 more generally we must obtain the effective rates of eqns. (22) and (23) by fitting the experimental transfer function to the data.

3.15.5. What is needed

We see that determining the true activation energies and pre-exponentials from observed effective rates requires some prior knowledge of the mechanism, reaction branching ratios, and surface coverages. We observe a distinct serial process. It is likely that the 10 kcal/mol step in H_2O and

HDO corresponds to hydrogen recombination. The other step is more difficult to assign. Our first guess was that 2.5 kcal/mol in H_2O corresponds to $H + O \rightarrow OH$, while an analysis of the HDO results suggests a 15 kcal/mol activation energy for H + OD.

We are reluctant to rely on these numbers until we have a more satisfactory qualitative understanding of the possible mechanisms, and can substantiate the approximations made. First we need careful mass balances to determine the ratio of hydrogen and oxygen desorption to reaction. This is difficult since the surface hydrogen coverage, oxygen desorption and water production rates are small. Most importantly, we need to know what fraction of the reactants on the surface are in the form of OH, and how quickly hydroxyl coverage responds to reactant modulation.

4. Summary

We have explored the oxidation of hydrogen to water on the Rh(111) surface over an extremely wide range of conditions and observed very different kinetic domains depending on temperature and reactant stoichiometry. Several techniques have been employed, most importantly modulated molecular beam reactive scattering using a new three-molecular-beam arrangement for linearized MBRS and control of coverage regimes.

4.1. Reaction order

The reaction does not show a simple global order in reactant pressure, fig. 3. As hydrogen flux is increases the steady-state reaction rate at first rises rapidly, then levels out. For high hydrogen flux the reaction is first order in oxygen, but for low hydrogen flux, the reaction rate first increases, then decreases as oxygen is increased. We have been able to model this qualitative behavior very well, fig. 4. We believe that with excess oxygen, all the hydrogen is converted to hydroxyl and none is left to go on to water.

4.2. Temperature dependence

We looked at temperatures from 400 to 1250 K. The peak reaction rate was around 650 K. At this temperature we estimate the hydrogen coverage to be on the order of 0.001 monolayer, and the oxygen coverage to be from a few tenths of a monolayer to saturation. Saturation with oxygen stops the reaction, either by converting all surface hydrogen to OH as mentioned above, or by blocking hydrogen adsorption, or both.

4.3. Titration of O_{ads} by H_2.

Quenching of the reaction by excess oxygen is also reflected in titration experiments, in which the surface is first dosed with oxygen, then the hydrogen beam is turned on and water production monitored, fig. 5. For small oxygen doses, water evolution is prompt. For larger oxygen doses, there is a delay before the reaction reaches its maximum. For oxygen doses near saturation at 650 K, the peak does not occur for several seconds.

4.4. Angular flux of H_2O

The angular distribution of the H_2O flux is cosine with respect to surface normal and the kinetics do not depend on angle. This is an indication that the product is equilibrated with the surface.

4.5. Low temperatures, nonlinearity

At a temperature of 520 K, the response of the reaction to a modulated hydrogen beam is nonlinear. The modulated product signal increases with continuous hydrogen flux, so overall product yield is not additive, fig. 11. The frequency response, or transfer function, does not obey superposition, and frequencies not present in the reactant modulation appear in the product response, fig. 10. The nonlinearity implies that the O + H step alone cannot be rate limiting under these conditions. Other reaction pathways, perhaps OH disproportionation, may become significant.

At still lower temperatures the reaction becomes difficult to control, showing hysteresis with

memory of previous reaction conditions, and coverage dependent rate constants. Possibly this is due to high oxygen coverages which are not at steady state and react very slowly to changing reaction conditions.

4.6. Multiple beam MBRS

We have introduced a useful extension of MBRS techniques, using multiple molecular beam sources to examine complex surface reactions over a wide range of coverage. Using two continuous, independently variable reactant beams we can choose and control steady state surface coverages. A weak modulated beam probes the kinetics by perturbing this steady state.

The ability to control reactant concentrations may be used to examine coverage dependent rate constants. Flexibility in choosing coverage regimes and use of isotopic substitution in multiple beams can allow different reaction pathways to emerge, as suggested by our low-temperature and HDO experiments. This may enable isolation of single elementary reaction steps in complex reaction networks.

Reactions can be moved from a nonlinear to linear regime by reducing the intensity of the modulated flux relative to continuous reactant flux. In the linear regime, deconvolution and other linear analysis methods may be applied to the data, and the sets of differential equations describing postulated mechanisms may be solved by perturbation techniques.

4.7. H_2O serial mechanism, oxygen coverage dependence

The transfer function for H_2O around the peak temperature of 650 K indicates a nearly linear, serial process with at least two steps. An Arrhenius construction for the temperature dependence of a two step fit gives $E_{a1} = 10.1 \pm 0.7$ kcal/mol, $A_1 = 10^{7.3}$ s^{-1} and $E_{a2} = 2.5 \pm 1.1$ kcal/mol and $A_2 = 10^{5.4}$ s^{-1}, fig. 13. The pressures of the continuous O_2 and H_2 beams were varied to examine the oxygen coverage dependence explicitly. The activation energies remain constant, but both pre-exponentials vary slightly with oxygen coverage.

4.8. Slow oxygen kinetics, dissolution, oscillation

This determination was complicated by long-term instability in oxygen coverage over tens of minutes. The reaction rate may oscillate, fig. 14. For continuous hydrogen and oxygen beam fluxes producing roughly half coverage of oxygen, we observed fluctuations in the Auger oxygen signal on the order of a few minutes. This instability was not seen at high or low oxygen coverages. These phenomena are on a much longer time scale than the rate constants for water production. The response to a modulated oxygen beam is also very slow compared to modulated hydrogen. This implies that oxygen coverage is not controlled entirely by water production, but by desorption, dissolution or other slow processes, or may indicate an unresolved slow step in the water mechanism.

4.9. Isotopic substitution, linearization

Using beams of both hydrogen and deuterium with oxygen, we looked at the production of H_2O, HDO and D_2O. With a large modulated beam flux we see strongly nonlinear responses. In particular, if we use continuous beams of deuterium and oxygen with modulated hydrogen, we see a strikingly asymmetric HDO waveform, and a negative modulation of the continuous D_2O background; fig. 15. The latter provides a measure of the extent to which the modulated beam perturbs the steady state surface coverages from the continuous beams. In both simulation and experiment on HDO we see the linearization of the response as the modulation, and the resulting perturbation of the surface coverages, is reduced.

4.10. Linearized HDO

The transfer function for linearized HDO is close to the single step arc, but additional steps are still evident. We obtain one rate with $A = 10^7$ s^{-1} and $E_a = 5.4 \pm 1.6$ kcal/mol, and a second with a similar pre-exponential but $E_a = 9.6 \pm 0.8$ kcal/mol; fig. 16. There was no difference between modulated H_2 and modulated D_2. Analysis of these apparent rates using a simple linearized

model suggests that the first step is hydrogen recombination with $E_a = 20$ kcal/mol, and that the second step may be H + OD → OH with $E_a =$ 15 kcal/mol. These assignments are highly speculative.

5. Conclusion

The reaction of hydrogen with oxygen on Rh(111) is surprisingly complex. We have explored a wide range of temperature and reactant fluxes, obtaining new data for high temperature, high oxygen coverage and low hydrogen coverage conditions. We have observed varied reaction regimes; linear, nonlinear, and possibly oscillatory, perhaps with different mechanisms. This complexity is also reflected in the various, sometimes contradictory, reports in the literature. We cannot yet reconcile all these results. A complete resolution of the mechanism may require the ability to monitor surface hydroxyl coverage on the same time scale as the water waveforms.

Acknowledgements

This work was supported in part by the Office of Naval Research, and by the NSF Materials Research Laboratory program at the University of Chicago (NSF-DMR-8819860).

References

[1] P.R. Norton, in: The Chemical Physics of Solid Surfaces and Heterogeneous Catalysis, Vol. 4, Eds. D.A. King and D.F. Woodruff (Elsevier, New York, 1982).
[2] T. Engel and H. Kuipers, Surf. Sci. 90 (1979) 181.
[3] G.B. Fisher and J.L. Gland, Surf. Sci. 94 (1980) 446.
[4] G.E. Mitchell and J.M. White, Chem. Phys. Lett. 135 (1987) 84.
[5] J.T. Yates, Jr., P.A. Thiel and W.H. Weinberg, Surf. Sci. 84 (1979) 427.
[6] P.A. Thiel, J.T. Yates, Jr. and W.H. Weinberg, Surf. Sci. 82 (1979) 22.
[7] P.A. Thiel, J.T. Yates, Jr. and W.H. Weinberg, Surf. Sci. 90 (1979) 121.
[8] J.T. Yates, Jr., P.A. Thiel and W.H. Weinberg, Surf. Sci. 82 (1979) 45.
[9] D.F. Padowitz and S.J. Sibener, J. Vac. Sci. Technol. A, in press.
[10] L.K. Verheij, M.B. Hugenschmidt, B. Poelsema and G. Comsa, Surf. Sci. 233 (1990) 209.
[11] M.A. Van Hove, W.H. Weinberg and C.-M. Chan, Low-Energy Electron Diffraction (Springer, Berlin, 1986).
[12] J.L. Gland, G.B. Fisher and E.B. Kollin, J. Catal. 77 (1981) 263.
[13] T. Germer and W. Ho, Chem. Phys. Lett. 163 (1989) 449.
[14] A.B. Anton and D.C. Cadogan, Surf. Sci. Lett. 239 (1990) L548.
[15] K.D. Gibson and S.J. Sibener, J. Chem. Phys. 88 (1988) 791.
[16] L.S. Brown and S.J. Sibener, J. Chem. Phys. 89 (1988) 1163.
[17] L.A. DeLouise and N. Winograd, Surf. Sci. 138 (1984) 417.
[18] D.S.Y. Hsu, M.A. Hoffbauer and M.C. Lin, Surf. Sci. 184 (1987) 25.
[19] H.-C. Chang and W.H. Weinberg, J. Chem. Phys. 66 (1977) 4176.
[20] T.W. Root, L.D. Schmidt and G.B. Fisher, Surf. Sci. 134 (1983) 30.
[21] K.A. Peterlinz, T. Curtiss and S.J. Sibener, to be published.
[22] M. Eiswirth, P. Möller, K. Wetzl, R. Imbihl and G. Ertl, J. Chem. Phys. 90 (1989) 510.
[23] M.R. Bassett and R. Imbihl, J. Chem. Phys. 93 (1990) 811.